Finite Reynolds number effects in the Bretherton problem

Dr. Matthias Heil

Department of Mathematics, University of Manchester

Oxford Road, Manchester M13 9PL, U.K.

Tel. +44 (0)161 275 5808

Fax. +44 (0)161 275 5819

email: M.Heil@maths.man.ac.uk

(Final version: June 1, 2001)

Physics of Fluids **13**, 2517–2521 (2001)

This paper investigates the effect of fluid inertia in the classical Bretherton problem in which a semi-infinite air finger displaces viscous fluid in a 2D channel. The governing free-surface Navier-Stokes equations are discretised by a finite element method and the system's behaviour is studied for capillary and Reynolds numbers in the ranges $0.05 < Ca < 5$ and $0 < Re < 280$, respectively. It is shown that at finite Reynolds number, a sequence of closed vortices develops in the recirculating flow region ahead of the bubble tip. The largest of these vortices is located near the bubble tip where it significantly affects the pressure distribution and leads to a noticeable increase in the overall pressure rise across the bubble tip. The underlying physical mechanisms are discussed in detail.

I. INTRODUCTION

The Bretherton problem in which a steadily propagating semi-infinite air finger (or a long air bubble) displaces viscous fluid in a 2D channel is a classical problem of fluid mechanics with applications in a wide variety of areas such as flow in porous media, multi-phase flows, chemical engineering and biomechanics.

Early experimental investigations by Fairbrother and Stubbs,[1] Taylor,[2] Cox[3] and Bretherton[4] showed that the thickness h_0^* of the film deposited on the wall by the propagating bubble decreases with a decrease in capillary number $Ca = U\mu/\sigma^*$, where U is the steady propagation speed of the bubble, and μ and σ^* are the fluid's viscosity and surface tension, respectively. Bretherton[4] carried out an asymptotic analysis for the limit $Ca \to 0$ and showed that $h_0 \sim Ca^{2/3}$ as $Ca \to 0$. His analysis was later refined by Park and Homsy[5] and extended to larger Ca by Ratulowski and Chang.[6] Cox[3] considered the limit of large Ca and showed that h_0^* approaches a finite value as Ca becomes large. For intermediate values of Ca, the problem needs to be studied numerically: Reinelt and Saffman[7] and Wassmuth, Laidlaw and Coombe[8] investigated the problem by finite difference approaches while most other numerical studies were performed either by boundary element methods (such as the studies by Lu and Chang,[9] Ingham, Ritchie and Taylor[10] and Halpern and Gaver[11]) or finite element methods (such as Shen and Udell[12] and Giavedoni and Saita[13]).

At low Reynolds number, the system's behaviour is governed by a balance between viscous and capillary forces near the bubble tip. Inertial effects have usually been assumed to be of minor importance in the problem. Consequently, only two of the numerical studies mentioned above included finite Reynolds number effects: Wassmuth, Laidlaw and Coombe,[8] whose study was mainly concerned with the effect of surfactants, performed their computations at a fixed Reynolds number of 20. Giavedoni and Saita[13] were the first to systematically investigate variations in the Reynolds number. They considered

Reynolds numbers of up to 70 and found that fluid inertia only led to moderate changes to the shape of the air finger and to the ultimate film thickness h_0^*. Thus their study seemed to confirm fluid inertia to be relatively insignificant in the problem.

The present paper re-investigates finite Reynolds number effects in the Bretherton problem over a larger range of Reynolds numbers. While confirming that fluid inertia has a relatively small effect on the ultimate film thickness h_0^* far behind the bubble tip, it is shown that finite Reynolds numbers have a significant effect on the flow field and the pressure distribution near the bubble tip. Fluid inertia is also shown to lead to a noticeable increase in the pressure rise across the bubble tip.

II. THE MODEL

Figure 1 shows a sketch of the Bretherton problem: inside a 2D channel of width $2H_0$, a positive bubble pressure p_b^* drives an air finger into a fluid of viscosity μ, density ρ and surface tension σ^*. The finger propagates at a steady speed U and leaves a film of thickness $h_0^* = h_0\ H_0$ behind. We non-dimensionalise all lengths by the channel half width H_0 and use a superscript star to distinguish dimensional quantities from their non-dimensional equivalents. As in previous investigations, we assume that the system remains symmetric about the channel's centreline and we only model the lower half of the domain. In a frame moving steadily with the velocity U of the bubble tip, the flow is described by the non-dimensional Navier-Stokes equations

$$Re\ u_j \frac{\partial u_i}{\partial x_j} = -\frac{\partial p}{\partial x_i} + \frac{\partial}{\partial x_j}\left(\frac{\partial u_i}{\partial x_j} + \frac{\partial u_j}{\partial x_i}\right) \tag{2.1}$$

and the continuity equation

$$\frac{\partial u_i}{\partial x_i} = 0, \tag{2.2}$$

where we have scaled the velocities with the bubble velocity, $u_i = u_i^*/U$, and have used the viscous pressure scale, $p = p^*/(\mu U/H_0)$. The Reynolds number is defined as $Re = UH_0\rho/\mu$. On the free fluid surface, whose outer unit normal we denote by $\mathbf{n}$, the fluid normal velocity vanishes,

$$\mathbf{u} \cdot \mathbf{n} = 0 \quad \text{on the air-liquid interface.} \tag{2.3}$$

We measure the fluid pressure p relative to the bubble pressure p_b. Then the dynamic boundary condition implies that

$$-pn_i + \left(\frac{\partial u_i}{\partial x_j} + \frac{\partial u_j}{\partial x_i}\right) n_j + \frac{1}{Ca}\,\kappa_f n_i = 0 \quad \text{on the air-liquid interface,} \tag{2.4}$$

where $\kappa_f = \kappa_f^* H_0$ is the non-dimensional interface curvature and the capillary number Ca is a non-dimensional measure of the bubble velocity. The no-slip condition on the channel walls requires that $\mathbf{u} = (-1, 0)$ at $x_2 = -1$. Far behind the bubble tip, the fluid remains stationary on the walls. In the moving frame of reference, this corresponds to the plug flow profile $\mathbf{u} = (-1, 0)$ as $x_1 \to -\infty$. The residual film thickness h_0 has to be determined as part of the solution and it determines the volume flux through the system. The Poiseuille velocity profile far ahead of the bubble tip, $\mathbf{u} = (-1 + \frac{3}{2}(1 - h_0)(1 - x_2^2), 0)$ as $x_1 \to \infty$, is then determined by overall continuity. The symmetry boundary condition on the channel's centreline requires that $u_2 = 0$ for $x_2 = 0$ and $x_1 > 0$.

Equations (2.1)-(2.4) were solved numerically by a finite element method, details of which can be found in reference [18]. Briefly, isoparametric Taylor-Hood elements were used to represent the pressure and velocity fields and the free surface position was resolved by Kistler and Scriven's[14] method of spines. The discretised equations were solved by a Newton-Raphson method in conjunction with an adaptive continuation technique to perform parameter variations. Demmel *et al.*'s[16] SuperLU solver with minimum degree ordering of the equations was used to solve the sparse linear systems. The discretisation typically extended from $x_L^1 = -35$ to $x_R^1 = 9$ and the standard discretisation used for the parameter studies presented below involved approximately 3100 degrees of freedom. Selected computations were repeated with a finer resolution of approximately 6300 degrees of freedom to check the mesh convergence of the results – see Fig. 2 below. At the standard resolution, a converged solution was typically obtained within a few minutes of CPU time on a DEC Alpha 433au workstation. Comparisons of the predictions against results available from the literature are presented below. A variant of the code was used in the more complicated problem in which the channel walls are elastic. For this case, a detailed comparison with Gaver *et al.*'s[17] zero Reynolds number BEM results was carried out and excellent agreement was obtained; see reference [18].

III. RESULTS

Giavedoni and Saita[13] investigated the effect of fluid inertia on the system's behaviour but only documented the variation of the residual film thickness h_0 with an increase in Reynolds number. They restricted themselves to Reynolds numbers in the range between 0 and 70 and somewhat arbitrarily regarded certain regions of parameter space as physically unrealisable. Figure 2 shows a comparison of their data with the data obtained from the present computations which were carried out over an extended range of Reynolds numbers. Also shown are the results obtained with a finer spatial resolution to confirm the mesh independence of the results. Figure 2 confirms Giavedoni and Saita's[13] prediction of a non-monotonic variation of h_0 with changes in Re: initially, an increase in Re reduces h_0; for larger values of Re, this behaviour is reversed. In all cases, the changes in h_0 are fairly moderate. This appears to confirm Giavedoni and Saita's[13] conclusion that finite Reynolds number effects are 'of minor importance in the present problem'.

Giavedoni and Saita[13] also reported that an increase in Re decreases the rate at which the film thickness approaches its final value h_0 as $x_1 \to -\infty$. This is confirmed by Fig. 3 which shows the streamlines and pressure distribution for a variety of Reynolds numbers and for $Ca = 0.05$. The figure also shows some significant changes to the flow field at finite Reynolds number which

Giavedoni and Saita[13] did not comment on: at finite Reynolds number, a closed vortex appears in the recirculating flow area ahead of the bubble tip. It is interesting to note that figure 6 in Wassmuth, Laidlaw and Coombe's[8] study shows a closed vortex in the velocity field ahead of the bubble at $Re = 20$. However, their study did not systematically investigate the effect of fluid inertia on the system's behaviour. Figure 3 shows that the size of the vortex increases with the Reynolds number and at $Re = 280$, it has grown to a length of more than three times the channel half width.

Note that the presence of a closed vortex implies the existence of a stagnation point (further away from the bubble tip) at which two streamlines intersect. The smooth continuation of the streamlines past this stagnation point suggests that a second vortex must be located ahead of the first one, etc. This should create a 'cat's eye' pattern of vortices as shown in the sketch in Fig. 4. Neither the stagnation point nor the other vortices can be detected in the streamline plots in Fig. 3 because the size of the vortices decays very rapidly with the distance from the bubble tip. The second vortex is already so small and hence close to the line along which $u_1 = 0$ (indicated by the dotted line in Fig. 4), that it can no longer be resolved by a streamline plot. However, it is possible to infer its presence from a plot of the magnitude of the transverse velocity u_2 whose sign we expect to change periodically with x_1, as shown in Fig. 4. Fig. 5 confirms this behaviour and identifies the position of the first stagnation point (for $Re = 140$ and $Ca = 0.05$) at $x_1 = 3.11$. The positive vertical velocities in the region ahead of this stagnation point are due to the displacement effect of the (much weaker and smaller) second vortex whose centre is located at $x_1 = 4.72$ where u_2 changes its sign again.

The pressure contours in Fig. 3 show that the increase in Reynolds number leads to significant changes in the fluid pressure distribution: the pressure rise across the bubble tip increases with an increase in Re and significant cross channel pressure gradients develop. Particularly noticeable is a pressure rise towards the bubble tip which affects the interface curvature via the dynamic boundary condition (2.4). This change in the pressure distribution is further analysed in Fig. 6, the top half of which shows the streamlines for $Re = 280$ and $Ca = 0.05$ on top of the contours of the absolute velocity, $|\mathbf{u}|$. At finite Reynolds number, streamline curvature creates a centrifugal pressure gradient away from the vortex centre. The centrifugal pressure rise is largest in the vicinity of the bubble tip where the strongly curved streamlines lie in a region of large absolute velocity. The 'carpet plot' of the corresponding pressure distribution (i.e. a plot of $p(x_1, x_2)$ versus x_1) in Fig. 6(b) shows that the pressure has a local minimum at the centre of the vortex. The inertial pressure rise towards the bubble tip can be seen to be of the same order of magnitude as the total pressure rise across the bubble. The inertial pressure variations in the other directions are much smaller: the large aspect ratio of the vortex leads to small curvature of the horizontal parts of the streamlines; the strongly curved streamlines at the right end of the vortex lie in regions of small absolute velocity.

Figure 7 shows that fluid inertia also has a significant effect on the distribution of vorticity in the flow. At zero Reynolds number, the distribution of vorticity ahead of the bubble tip is dominated by the linear variation imposed by the oncoming Poiseuille flow. Behind the bubble tip, the vorticity rapidly tends to zero. At finite Reynolds number, the recirculating flow ahead of the bubble tip advects vorticity towards the channel's centreline and leads to a noticeable distortion of the vorticity field. Furthermore, the vorticity decays much more slowly behind the bubble tip.

In practical applications, one of the most important parameters in the problem is the pressure required to drive the air finger at a given speed. Far ahead of the bubble, the Poiseuille flow induces a constant negative pressure gradient. Therefore, the driving pressure has to be determined as the difference between the bubble pressure p_b and the fluid pressure at a fixed distance ahead of the bubble tip. At zero Reynolds number, the cross channel pressure gradient remains small throughout the domain and the fluid pressure $p_{tip} = p(0, 0)$ at the bubble tip provides an adequate reference value for the driving pressure difference. The inertial pressure rise towards the bubble tip means that, at finite Reynolds number, this is no longer the case. Figure 8 shows the pressure distribution $p(x_1, x_2 = -1)$ along the wall for various Reynolds numbers and for $Ca = 0.05$. The figure shows that an increase in Reynolds number significantly increases the pressure required to drive the fluid at a given speed. A comparison with Fig. 6 shows that the increase of the driving pressure difference is significantly larger than the corresponding increase in $p_b - p_{tip}$ since p_{tip} is no longer representative of the 'average' fluid pressure ahead of the bubble tip.

Figure 9 represents the pressure distribution $p(x_1, x_2 = -1)$ along the wall for various capillary numbers and for $Re = 280$. The figure shows that the pressure variations due to fluid inertia are largest at small capillary number. This is consistent with the above observations: for large Ca, the residual film thickness h_0 exceeds the value at which a recirculating flow area develops ahead of the bubble. Therefore, at large Ca the inertial pressure variations caused by the centrifugal pressure gradient in the closed vortex are absent. Furthermore, at large Ca, all fluid approaches the bubble tip from the right (in the moving frame of reference) but the fluid velocity near the channel's centreline is smaller than that near the moving wall. In the vicinity of the bubble tip, the oncoming fluid is accelerated and deflected around the bubble tip until it reaches the region of constant film thickness where all fluid moves with unit velocity. At finite Reynolds number, fluid inertia resists this acceleration and it takes longer for the film thickness to approach its ultimate value h_0 as $x_1 \to -\infty$. This makes the front part of the air finger more slender and decreases the radius of curvature of the bubble tip.

Conversely, at large Re and small Ca the pressure variations near the bubble tip are dominated by the centrifugal pressure gradients created by the closed vortex which lead to the noticeable local pressure minimum ahead of the bubble tip shown in Fig. 9. Furthermore, at small Ca, only a fraction of the fluid is advected into the thin film region behind the bubble tip and needs to be accelerated to unit velocity. Therefore, the overall inertial resistance to this acceleration is relatively small and the rate at which the film thickness approaches its ultimate value h_0 as $x_1 \to -\infty$ only decreases slightly with an increase in Reynolds number.

Finally, we note the small variations in the pressure gradient far ahead of the bubble with variations in Re and Ca. These are caused by the adjustment of the Poiseuille velocity profile to the variations in h_0. Figures 8 and 9 show that these changes to the pressure distribution are insignificant compared to the inertial pressure variations near the bubble tip.

IV. DISCUSSION

The results reported in the previous section show that fluid inertia can play an important role in the Bretherton problem even though some global quantities, such as the residual film thickness h_0, only vary slightly with an increase in Reynolds number. The changes to the flow field ahead of the bubble tip will affect any advection/diffusion processes in the flow. This is of particular importance for problems in which the dynamics of the air-liquid interface are affected by adsorption/desorption of surfactant from the bulk of the fluid. If the Peclet number of the advection/diffusion process in the bulk of the fluid is sufficiently large then the changes to the velocity field at finite Reynolds number could have a profound effect on the system's behaviour.

The results showed that inertial effects are most significant at large Reynolds number and small capillary number. This raises the question if sufficiently large values of Re/Ca (e.g. $Re/Ca = 5600$ for the flow field analysed in Fig. 6) are realisable in the typical experimental setups and in practical applications. Expressing Re/Ca in terms of the physical parameters shows that $Re/Ca = \rho\sigma^* H_0/\mu^2$ which indicates that the fluid viscosity μ has the strongest effect on its variations. To illustrate typical orders of magnitude for Re/Ca, consider an experiment in which water ($\rho = 1$ g/cm^3, $\mu = 0.01$ g/(cm sec), $\sigma^* = 20$ dyn/cm) is displaced by an air finger: for these parameter values, we only require a channel width of $2H_0 = 0.05$ cm to obtain a ratio of $Re/Ca = 5000$. Note that most experiments were performed in channels (or tubes) of much greater width. This shows that Bretherton flows in which finite Reynolds number effects are important are easily realisable experimentally. Giavedoni and Saita's[13] restrictions on the 'practically feasible' parameter range therefore appears to be unnecessary.

The size of the inertial pressure variations in the rigid channel, observed in the present study, suggests that the effect of fluid inertia might be even more significant in situations where the channel walls are allowed to deform in response to the fluid pressure. This is confirmed by Heil's[18] study of the propagation of an air finger into a flexible walled channel, which shows that in this system, inertial effects become important at much smaller values of Re and Re/Ca than in the rigid walled system.

ACKNOWLEDGEMENTS

The author would like to thank Dr. Andrew Hazel and two anonymous referees for their valuable comments which helped to significantly improve an earlier version of the manuscript. Financial support from the EPSRC is acknowledged.

---

[1] F. Fairbrother and A.E. Stubbs, "Studies in Electroendosmosis. Part VI. The bubble-tube method of measurements," J. Chem. Soc. **1**, 527-529 (1935).

[2] G.I. Taylor, "Deposition of a viscous fluid on the wall of a tube," Journal of Fluid Mechanics **10**, 161-165 (1961).

[3] B.G. Cox, "On driving viscous fluid out of a tube," Journal of Fluid Mechanics

14, 81-96 (1962).

[4] F.P. Bretherton, "The motion of long bubbles in tubes," Journal of Fluid Mechanics **10**, 166-188 (1961).

[5] C.-W. Park and G.M. Homsy, "Two-phase displacement in Hele Shaw cells: theory," Journal of Fluid Mechanics **139**, 291-308 (1984).

[6] J. Ratulowski and H.-C. Chang, "Transport of gas bubbles in capillaries," Physics of Fluids A **1**, 1642-1655 (1989).

[7] D.A. Reinelt and P. Saffman "The Penetration of a Finger into a Viscous Fluid in a Channel and Tube," SIAM Journal of Scientific and Statistical Computing **6**, 542-561 (1985).

[8] F. Wassmuth, W.G. Laidlaw and D.A. Coombe, "Calculation of interfacial flows and surfactant redistribution as a gas/liquid interface moves between two parallel plates," Physics of Fluids A **5**, 1533-1548 (1993).

[9] W.-Q. Lu and H.-C. Chang, "An Extension of the Biharmonic Boundary Integral Method to Free Surface Flow in Channels," Journal of Computational Physics **77**, 340-360 (1988).

[10] D.B. Ingham, J.A. Ritchie and C.M. Taylor, "The motion of a semi-infinite bubble between parallel plates," ZAMP **43**, 191-206 (1992).

[11] D. Halpern and D.P. Gaver, "Boundary Element Analysis of the Time-Dependent Motion of a Semi-infinite Bubble in a Channel," Journal of Computational Physics **115**, 366-375 (1994).

[12] E.I. Shen and K.S. Udell, "A Finite Element Study of Low Reynolds Number Two-Phase Flow in Cylindrical Tubes," ASME Journal of Applied Mechanics **52**, 253-256 (1985).

[13] M.D. Giavedoni and F.A. Saita, "The axisymmetric and plane cases of a gas phase steadily displacing a Newtonian liquid – A simultaneous solution of the

governing equations," Physics of Fluids **9**, 2420-2428 (1997).

[14] S.F. Kistler and L.E. Scriven, "Coating Flows." In: "Computational Analysis of Polymer Processing," Pearson, J.R.A. and Richardson, S.M. (eds.); Applied Science Publishers, London (1983).

[15] K.J. Ruschak, "A Method for Incorporating Free Boundaries with Surface Tension in Finite Element Fluid-Flow Simulations". International Journal for Numerical Methods in Engineering **15**, 639-648 (1980) .

[16] J.W. Demmel, S.C. Eisenstat, J.R. Gilbert, X.S. Li and J.W.H. Liu, "A supernodal approach to sparse partial pivoting," SIAM Journal on Matrix Analysis and Applications **20**, 720-755 (1999).

[17] D. P. Gaver, D. Halpern, O.E. Jensen and J. Grotberg, "The steady motion of a semi-infinite bubble through a flexible walled channel," Journal of Fluid Mechanics **319**, 25-56 (1996).

[18] M. Heil, "Finite Reynolds number effects in the propagation of an air finger into a liquid-filled flexible-walled channel," Journal of Fluid Mechanics **424**, 21-44 (2000).

FIGURES:

hierher

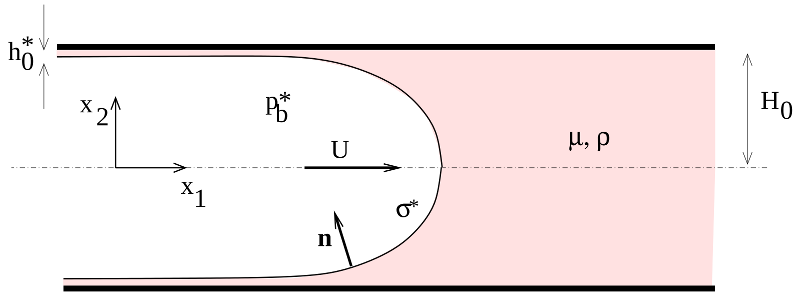

FIG. 1. Sketch of the model problem: an air finger propagates into a fluid-filled two-dimensional channel.

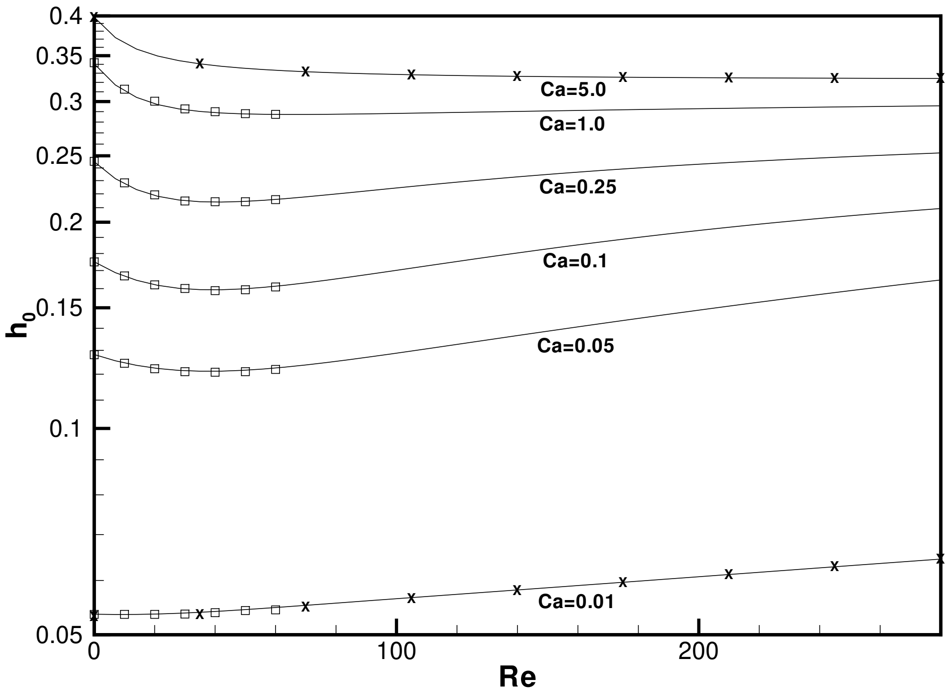

FIG. 2. The dimensionless film thickness h_0 versus the Reynolds number Re for various values of the capillary number Ca. The square markers represent Giavedoni and Saita's data, the crosses represent data obtained with a finer spatial resolution.

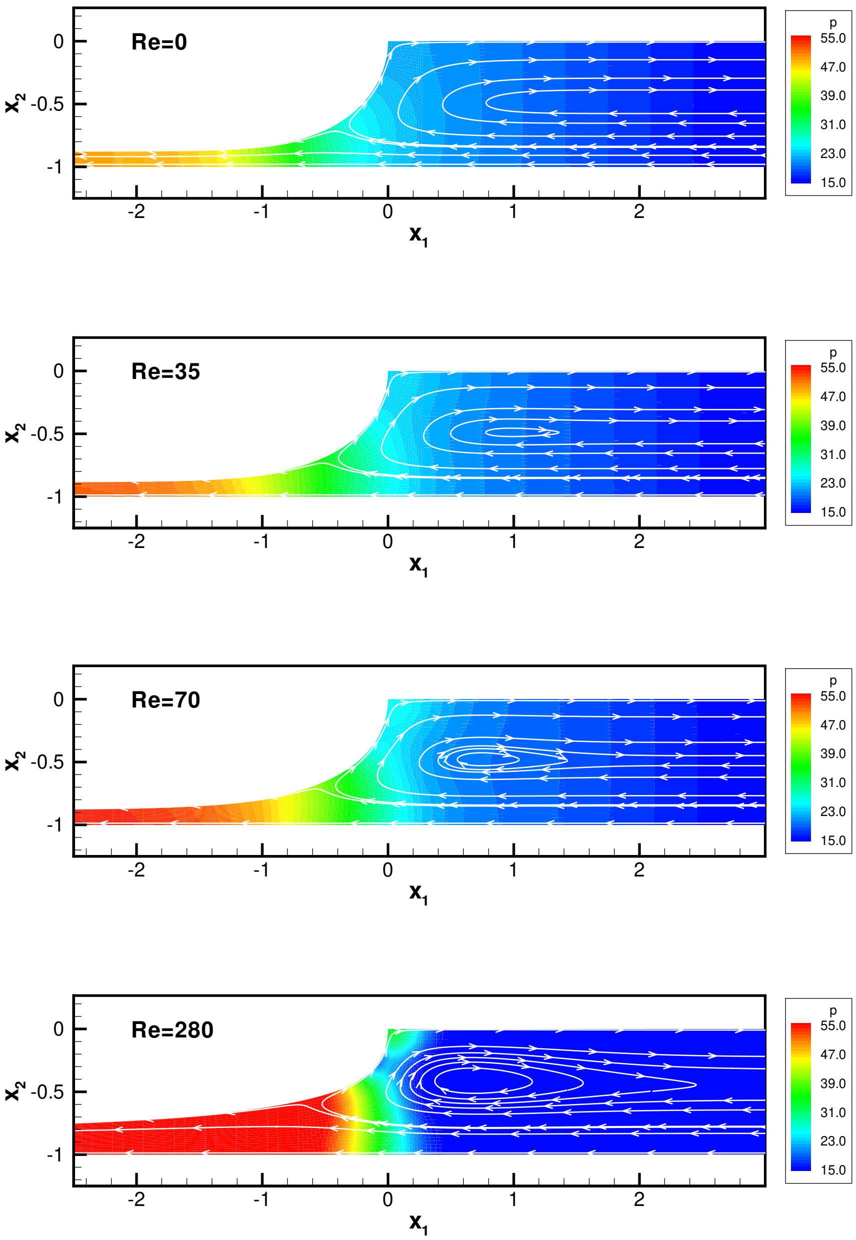

FIG. 3. The flow field and the pressure distribution at various Reynolds numbers for $Ca = 0.05$. At finite Reynolds number, a closed vortex appears ahead of the bubble tip and significant cross channel pressure gradients develop.

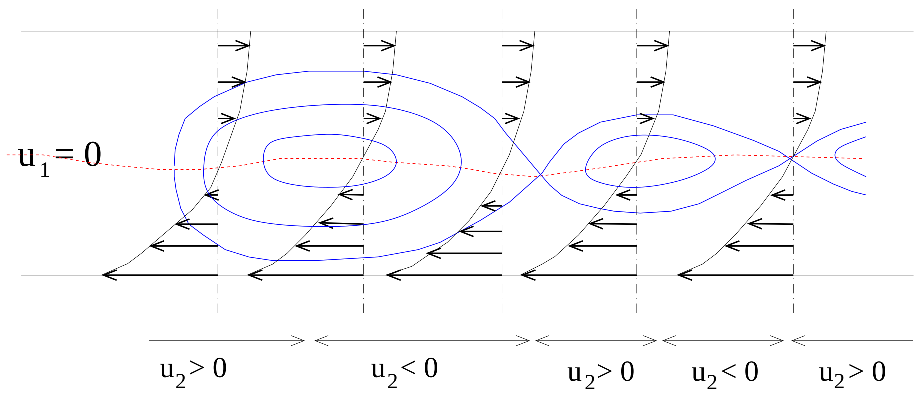

FIG. 4. Sketch of the 'cat's eye' pattern of vortices ahead of the bubble tip. The dotted line indicates the line along which $u_1 = 0$ and connects the stagnation points between the vortices. Note that all vortices have the same sense of rotation and that the sign of u_2 varies periodically with x_1.

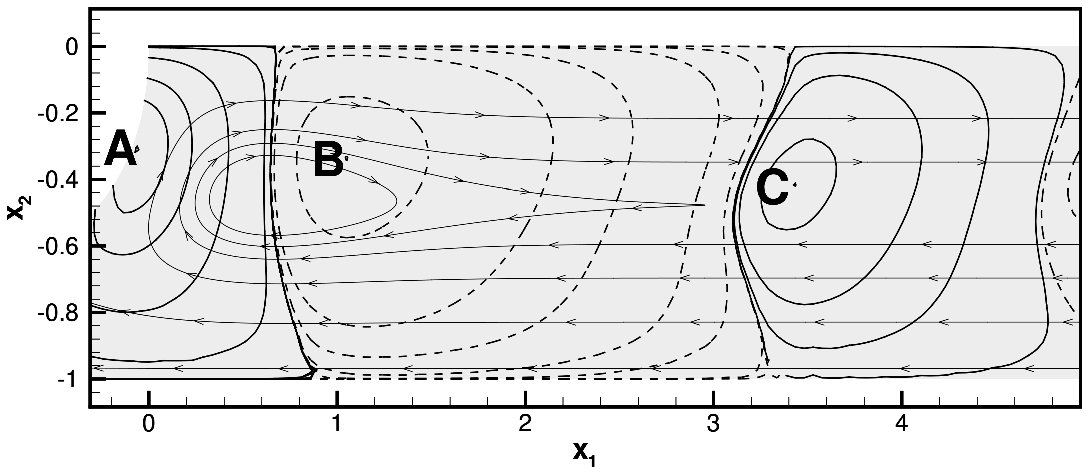

FIG. 5. Streamlines (thin) and isolines of the transverse velocity u_2 (thick) for $Re = 140$ and $Ca = 0.05$. Broken lines indicate negative values. The extrema of u_2 are $u_2(A) = 3.05 \times 10^{-1}$, $u_2(B) = -2.04 \times 10^{-2}$, $u_2(C) = 1.59 \times 10^{-5}$.

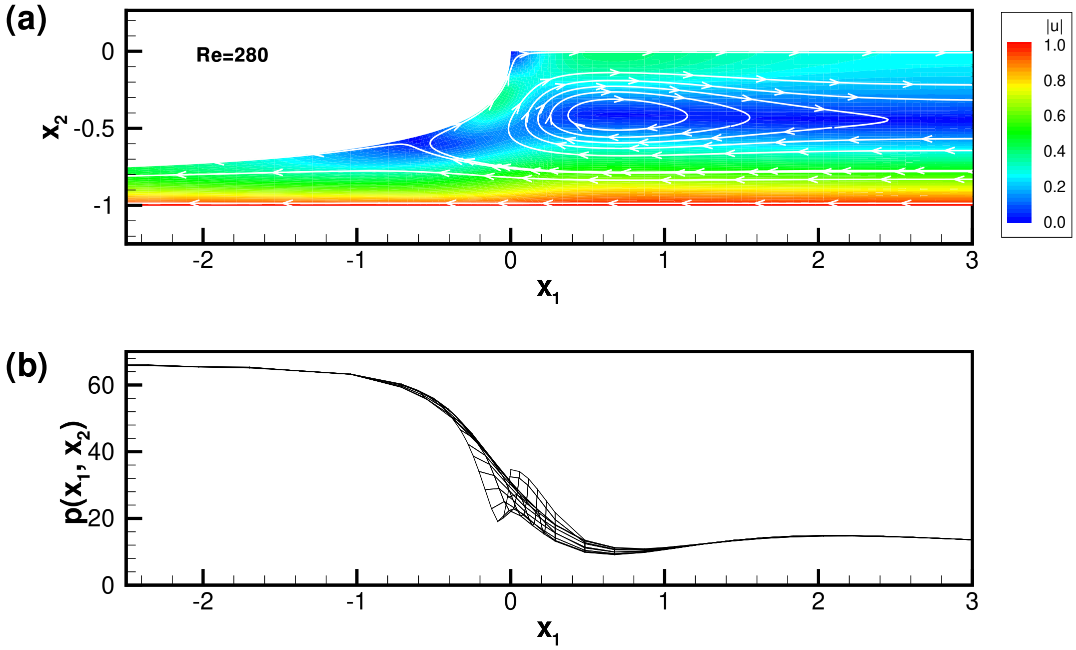

FIG. 6. The flow field and the pressure distribution at $Ca = 0.05, Re = 280$. (a) Streamlines on top of the contours of the absolute velocity, $|\mathbf{u}|$. (b) The corresponding pressure distribution, shown as a carpet plot, $p(x_1, x_2)$ versus x_1.

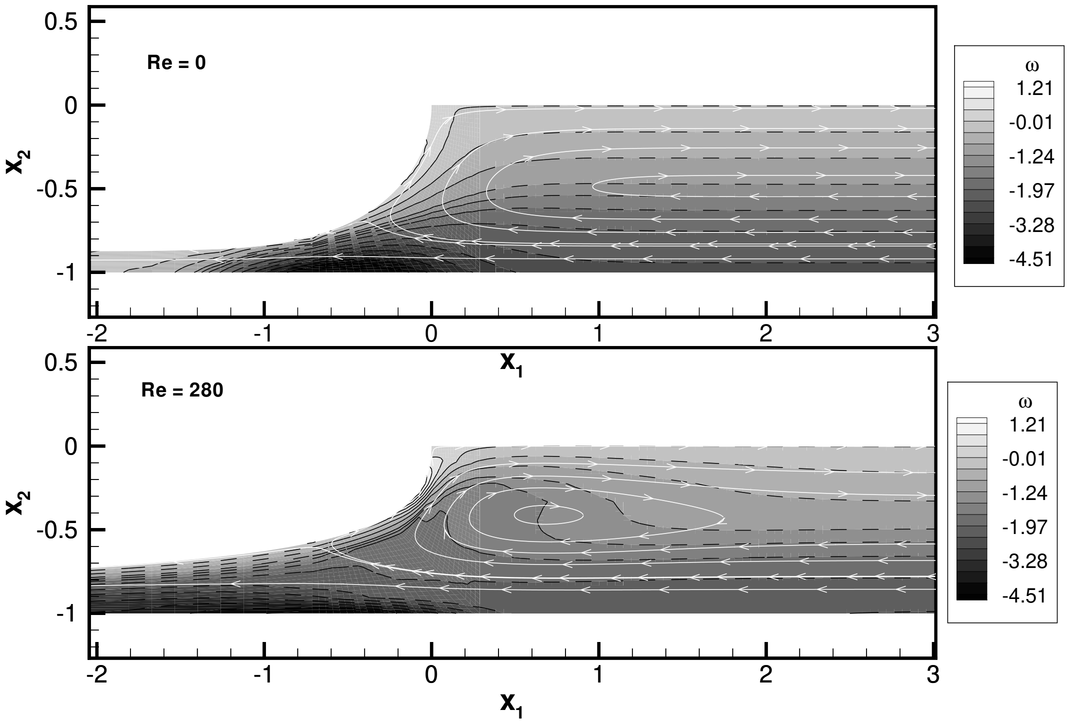

FIG. 7. The flow field and the vorticity distribution for $Ca = 0.05$. (a) $Re = 0$ (b) $Re = 280$.

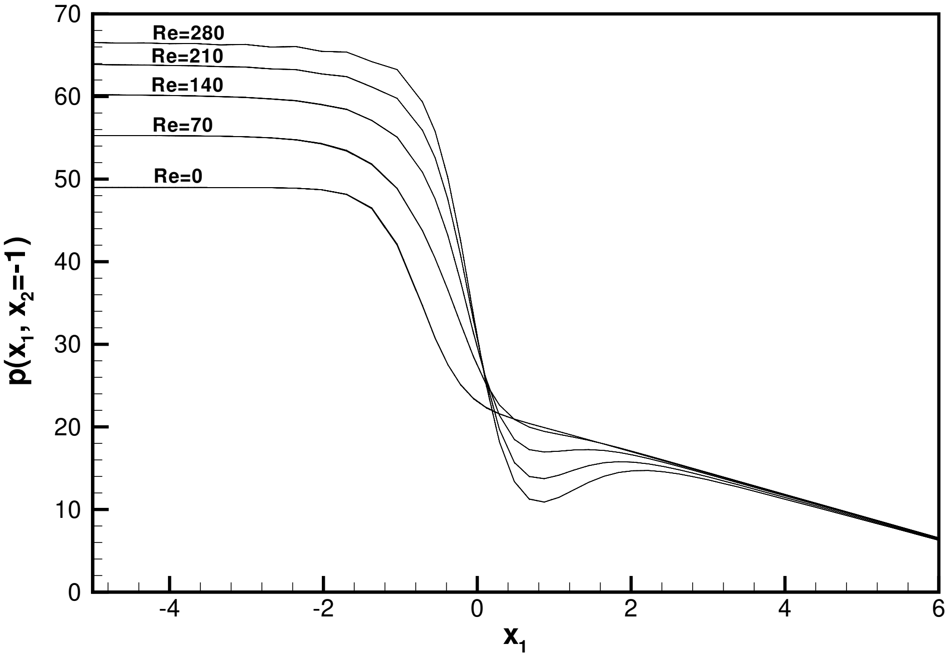

FIG. 8. The fluid pressure $p(x_1, x_2 = -1)$ along the wall for various Reynolds numbers Re and for $Ca = 0.05$.

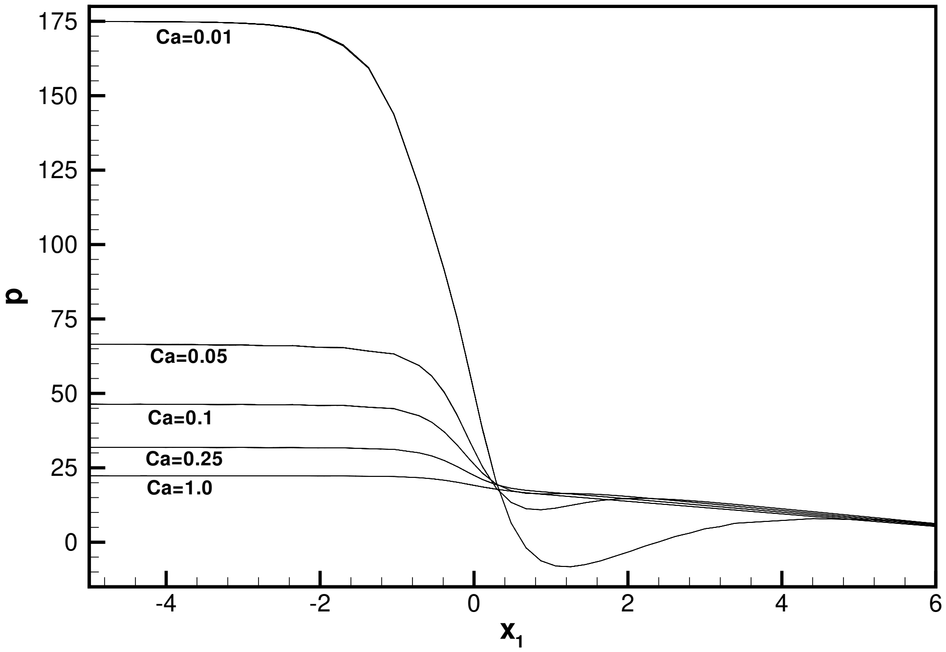

FIG. 9. The fluid pressure $p(x_1, x_2 = -1)$ along the wall for various capillary numbers Ca and for $Re = 280$.